Title

The Connection between Resonances and Bound States in the Presence of a Coulomb Potential

Permalink

https://escholarship.org/uc/item/4tz8h8r7

Journal

The Journal of Physical Chemistry A, 123(1)

ISSN

1089-5639

Authors

Lucchese, RR
Rescigno, TN
McCurdy, CW

Publication Date

2019-01-10

DOI

10.1021/acs.jpca.8b10715

Peer reviewed

The connection between resonances and bound states in the presence of a Coulomb potential

R. R. Lucchese,[*,†] T. N. Rescigno,[†] and C. W. McCurdy[†,‡]

†*Chemical Sciences Division, Lawrence Berkeley National Laboratory, Berkeley CA 94720*
‡*Department of Chemistry, University of California, Davis, CA 95616 USA*

E-mail: rlucchese@lbl.gov

Abstract

The connection between resonant metastable states and bound states with changing potential strength in the presence of a Coulomb potential is fundamentally different from the case of short-range potentials. This phenomenon is central to the physics of dissociative recombination of electrons with molecular cations. Here, it is verified computationally that there is no direct connection between the resonance pole of the S-matrix and any pole in the bound state spectrum. A detailed analysis is presented of the analytic structure of the scattering matrix in which the resonance pole remains distinct in the complex k-plane while a new state appears in the bound state spectrum. A formulation of quantum defect theory is developed based on the scattering matrix which nonetheless exposes a close analytic relation between the resonant and bound state poles, and thereby reveals the connection between quantum defect theory and analytic S-matrix theory in the complex energy and momentum planes. One-channel and multi-channel versions of the expressions with numerical examples for simple models are given and the formalism is applied to give a unified picture of *ab initio* electronic structure and scattering calculations for e-O_2^+ and e-H_2^+ scattering.

1 Introduction

A central concept of collision theory is idea that bound states can become metastable states with finite lifetimes (scattering resonances) and vice versa as the strength of the interaction potential is varied, and this is the subject of classic textbook discussions of scattering theory.[1,2] This phenomenon is well known in electron-molecule scattering, where it provides the mechanism for dissociative attachment of electrons to molecules and dissociative recombination (DR) of electrons to molecular cations,

$$AB^+ + e^- \to AB^* \to A + B. \tag{1}$$
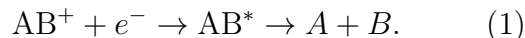
This process has of course been the subject of many theoretical studies.[3–10] In these treatments a recurring theme is the connection of the lifetime of the relevant autoionizing electronic states to the spectrum of the electronic Hamiltonian at molecular geometries where the corresponding bound states of the molecule appear.

The idea that the two states are continuously connected is almost always implicit in these treatments, even though Domcke[11] noted that no such continuous connection exists in a beautiful study in 1983 that seems to have received little attention. At the time of that study it had been known at least since 1977 that the width, and therefore the lifetime, of an autoionizing state is finite even when the real part of its energy is zero, as Miller and Morgner[12] showed on the basis of a semiclassical analysis.

Not withstanding this context, remarkable progress has been made in decades of work on the treatment of dissociative recombination by the application of quantum defect theory[13–15] in many studies and calculations of dissociative recombination cross sections,[4,6,9,10,16] which owe a great deal to the foundational work of Giusti[3] in 1980. In these applications quantum defect theory makes a powerful and useful connection between the Rydberg states of a neutral molecule and electron-ion scattering described by the S-matrix at (real-valued) low energies. However, Domcke's analysis[11] suggests that in general there is no direct analytical connection between the the poles of the S-matrix corresponding to autoionizing states and those corresponding to the appearance of new bound states with which they might be associated, and therefore raises the question of how to reconcile quantum defect theory with the formal theory of the analytic structure of the S-matrix.

Here we analyze the connection between resonance states in the presence of Coulomb potentials, and provide a formulation of quantum defect theory for both one-channel and multi-channel cases that unifies it with analytic S-matrix theory. The working equations of the present formulation are somewhat different, in particular for the multichannel case, from those of the traditional formulation, but they give the same physical states at real values of the energy while offering a complete analytic continuation into the complex energy and momentum planes. We demonstrate this form of the theory for exactly solvable one- and three-channel models. We also exploit the complex pole structure of this theory to give a unified picture of the results of *ab initio* electronic structure calculations of the quantum defects as a function of internuclear distance and the S-matrices calculated in *ab initio* electron scattering calculations for the cases of electron scattering from the O_2^+ and H_2^+ ions.

In a separate, but related, context, several methods[17–20] have been proposed for computing the lifetimes of resonances in electron scattering from *neutral* molecules by converting them into bound states by the addition of an attractive Coulomb potential, and then analytically
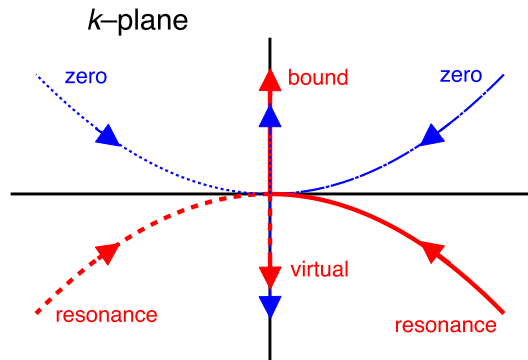

Figure 1: Sketch of the classic behavior in the momentum plane of resonance and bound state poles and the corresponding zeros of the S-matrix with varying potential strength in scattering from a short range potential with non-zero angular momentum. The red lines correspond to the trajectories of the poles and the blue lines correspond to the trajectories of the zeros.

continuing the resulting bound state energies as functions of the effective charge back to zero charge. These procedures have had apparent success by treating the resonance and bound pole trajectories explicitly as though they were related to one another as in the classic case of scattering from short range potential. In that case resonance and bound state poles interconvert as the potential strength is varied in the way sketched in Fig. 1, where there are two resonances or two bound states (for nonzero angular momentum) that interconvert as a function of potential strength, λ, with a characteristic square root branch behavior,[1,2] $k_{\text{pole}} \approx \pm i\, a(\lambda - \lambda_0)^{1/2}$. It has been pointed out recently that this procedure is not well founded because the pole corresponding to a resonance in the presence of a Coulomb potential cannot move continuously to become a bound state pole.[21] However no answer has been given to the question of why such an analytic continuation procedure involving the addition of Coulomb potentials can ever be apparently successful.

In this paper we seek to shed some light on these questions. We begin in Section 2 with an analytically solvable model problem that we analyze in detail without making the approxi-

2

mations specific to small values of the scattering momentum, k, that Domcke used in his original study. That analysis allows us to construct a somewhat more explicit mathematical and numerical picture of the properties and motion of the poles of the S-matrix that we suggest reflects the more general physical situation. In Section 3 we develop an explicit connection of the poles of the S-matrix to quantum defect theory for single-channel problems. We discuss how to parameterize the pole and zero structure and fit computed data. We then give an example which can be solved exactly in the complex k-plane as well as a real molecular example, the $^1\Sigma_u^+$ resonance in e-O_2^+, where we parameterize the resonance based on bound state and scattering calculations at real energies. In Sec. 4 we give the analogous expressions for multichannel systems and consider both an exactly solvable model problem and an *ab initio* treatment of the $^1\Sigma_g^+$ resonance in e-H_2^+. Finally, in Sec. 5 we give some concluding remarks.

2 Interplay of resonances and bound states in the presence of a Coulomb potential

We will begin by analyzing bound states and resonance poles of the S-matrix for a square-well plus attractive Coulomb potential with the product of the projectile and target charges being $Z = -1$,

$$V(r) = \begin{cases} -V_0 + Z/r & r \le r_0 \\ Z/r & r > r_0. \end{cases} \quad (2)$$

The plot of this potential in Fig. 2 reveals immediately why a resonance trapped behind the barrier will have a finite width as the well is deepened by increasing V_0 to the point where it has zero energy. Unlike the case of any short range potential, where the centrifugal barrier will be of infinite range at zero energy, the barrier in this case is of finite width at $E = 0$.

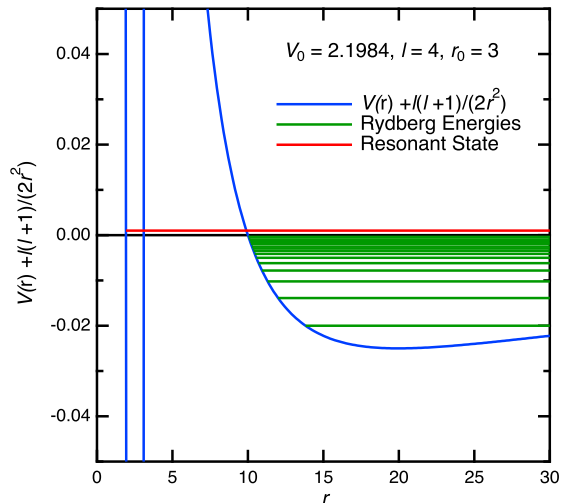This is a simple example of the class of "short

Figure 2: Potential for the radial square well plus an attractive Coulomb potential as defined in Eq. (2) with $l = 4$, $Z = -1$, $r_0 = 3$ for $V_0 = 2.1984$. The energy levels of the Rydberg states are given by the green horizontal line and the red line indicates the energy of a near threshold scattering resonance illustrating that the width of the tunneling barrier is finite as the resonance energy approaches zero due to the presence of the strong Coulomb potential outside the range of the attractive square-well potential.

range plus Coulomb" problems that are familiar from standard textbook discussions of Coulomb scattering. The partial wave S-matrix for the complete scattering problem can be written[1] in terms of the Coulomb phase shift, $\eta_l = \arg \Gamma(l + 1 + in)$ with $n \equiv Z/k$,

$$S_l = e^{2i(\eta_l + \delta_l)} = \frac{\Gamma(l + 1 + in)}{\Gamma(l + 1 - in)} S_l^{\mathrm{SR}} . \quad (3)$$

The phase shift due to the addition of the short-range potential determines the short-range S-matrix, $S_l^{\mathrm{SR}} = \exp(2i\delta_l)$, and it has poles at the bound states and resonances of the system. The properties of the Γ function in the complex plane result in the Coulomb factor, $\exp(2i\eta_l)$, having no poles except at the bound states of the pure Coulomb potential.

The short-range S-matrix is determined by matching the solutions of the radial Schrödinger equation (atomic units throughout unless oth-

3

erwise indicated),

$$\left[-\frac{1}{2}\frac{d^2}{dr^2} + V(r) + \frac{l(l+1)}{2r^2} \right]\psi(r) = E\psi(r) \tag{4}$$

for $r < r_0$ and $r > r_0$ in terms of the Coulomb functions given in Appendix A,

$$\psi = \begin{cases} A\,F_l(K,r) & r \leq r_0 \\ H_l^-(k,r)e^{-il\pi/2} \\ \quad -S_l^{\mathrm{SR}}(k)\,H_l^+(k,r)e^{+il\pi/2} & r > r_0 \end{cases} \tag{5}$$

with

$$K \equiv \left(k^2 + 2V_0\right)^{1/2}. \tag{6}$$

We find the short-range S-matrix

$$S_l^{\mathrm{SR}}(k) = e^{-il\pi}\frac{\mathbb{W}_{r_0}[F_l(K,r), H_l^-(k,r)]}{\mathbb{W}_{r_0}[F_l(K,r), H_l^+(k,r)]} \tag{7}$$

where $\mathbb{W}_{r_0}[f,g]$ is the Wronskian,

$$\mathbb{W}_{r_0}[f,g] = \left.\left(\frac{df}{dr}g - \frac{dg}{dr}f\right)\right|_{r0}. \tag{8}$$

This expression can be simplfied and written in terms of Whittaker functions[22] as

$$S_l^{\mathrm{SR}}(k) = \frac{D_l(-k)}{D_l(k)} \tag{9}$$

with the denominator function,

$$D_l(k) = e^{-i(l+1)\pi/2}\,\Gamma(l+1+in) \\ \times \mathbb{W}_{r_0}\left[M_{+iZ/K,l+1/2}(+2iKr), W_{-in,l+1/2}(-2ikr)\right], \tag{10}$$

The Wronskian in Eq.(10) can be evaluated analytically in terms of Whittaker functions with different arguments.

Some aspects of the analytic structure of the S-matrix in Eq.(9) are apparent on inspection. The Whittaker function $M_{\kappa,\mu}(z)$ is a single valued function, but $W_{-in,l+1/2}(-2ikr)$ is many-valued because it has a logarithmic singularity at $k = 0$ and an associated branch cut which we will take to lie on the negative imaginary k axis. With that convention the numerator and denominator of $S_l^{\mathrm{SR}}(k)$ satisfy a reflection rela-
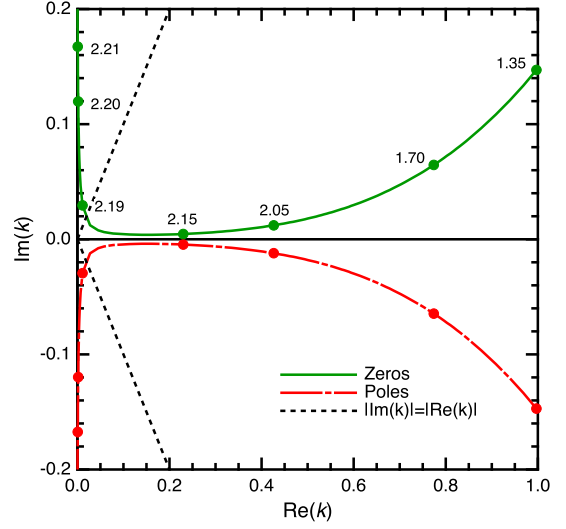

Figure 3: Resonance pole trajectory (red) and zeros of S-matrix (green) for square-well plus Coulomb potential with $l = 4$, $Z = -1$, $r_0 = 3$ for $V_0 = 1.35$ to 2.22. The labels next to some selected points indicate the well depth at that point. The dashed lines (black) indicate where $\mathrm{Re}(E) = 0$.

tion

$$D_l(-k^*) = D_l(k)^*. \tag{11}$$

This is the reflection relation satisfied in general by the Jost function,[1,2] but here there is an important subtlety. This relation arises explicitly in Eq.(10) because of (1) the analytic continuation relation[22] satisfied by the Whittaker function, $M_{\kappa,\mu}(ze^{\pm i\pi}) = \pm ie^{\pm i\pi\mu}M_{-\kappa,\mu}(z)$, and (2) the fact that $W_{-in,l+1/2}(-2ikr)$ satisfies the same reflection relation with our choice of branch cut convention. The branch cut in $D_l(k)$ on the negative imaginary k-axis is a branch cut of $S_l^{\mathrm{SR}}(k)$, which also has a branch cut on the positive imaginary axis associated with its numerator, $D_l(-k)$. These branch cuts of the S-matrix on both the positive and negative imaginary k-axes will be seen below to play an important role in the trajectories of the resonance poles of $S_l^{\mathrm{SR}}(k)$.

The second observation we can make immediately about the S-matrix is that it has a set of zeros and poles that are fixed and do not move as functions of the potential strength, V_0. The Γ function prefactor $\Gamma(l+1-in)$ in the numerator of $S_l^{\mathrm{SR}}(k)$ has poles at $k = iZ/(m+l+1)$ for in-
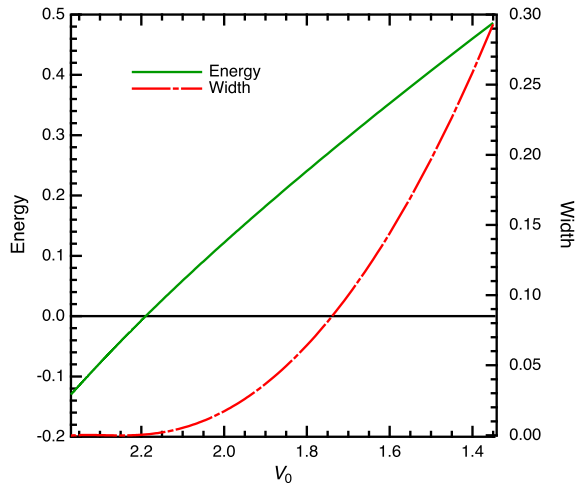
4

Figure 4: Resonance energy (green) and width (red) as a function of V_0 for square-well plus Coulomb potential with $l = 4$, $Z = -1$, $r_0 = 3$.

teger $m \geq 0$, while the factor in the denominator $\Gamma(l+1+in)$ has poles at $k = -iZ/(m+l+1)$. For $Z < 0$ that means that the numerator has poles on the negative imaginary k-axes that do not move with changing V_0 or r_0. It also has fixed zeros at the mirror images of those locations on the positive imaginary k axis.

The Gamma function factor $\Gamma(l + 1 + in)$ in $D_l(k)$ has no zeros in the complex k-plane, so it does not produce any poles of S. So the zeros of the Wronskian in Eq.(10) are the physically relevant poles and zeros of $S(k)$, and we now turn our attention to them.

In Fig. 3 we show the trajectory of the zeros and poles of S^{SR} in the complex k-plane as a function of the well depth, V_0, for the one-dimensional problem defined by Eqs. (2) and (4), with $l = 4$, $Z = -1$, and $r_0 = 3$. This figure does not include the poles due to the bound Coulomb states which are on the positive imaginary k-axis. We can see that as the well is made deeper, the pole approaches the origin, but then it moves further away from the real axis and does not become a bound state. The corresponding zero of the S-matrix moves upwards near the positive imaginary k axis where it can perturb the positions of the poles in the S matrix which occur on the positive imaginary k-axis.

In Fig. 4 we can see that in this problem, with high angular momentum, the width of the

resonance changes rapidly as the resonance approaches zero energy. The real part of the resonance energy is nearly a linear function of the potential strength V_0 and goes through zero at $V_0 = 2.1894$, while the width remains finite at that point.
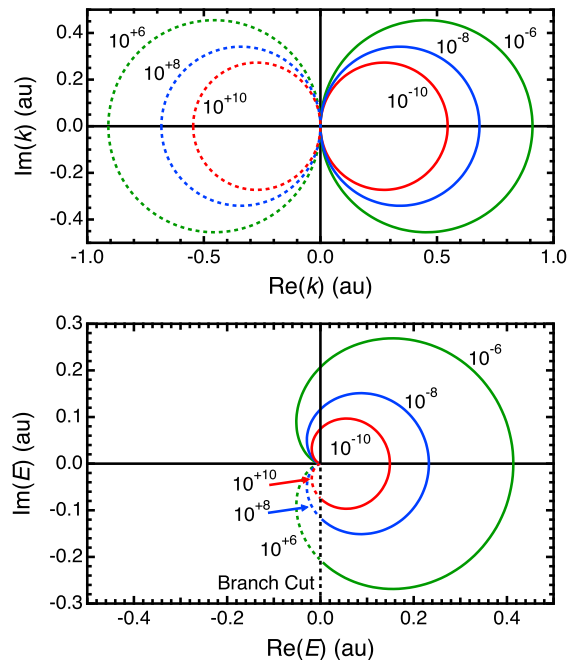

Figure 5: Value of $|Q|$ as defined in Eq. (21) for $Z = -1$. Upper panel is in the complex k-plane and the lower panel is in the complex E-plane. Note that, in the plots of various functions in the E-plane, for a given E we select the corresponding k needed to compute Q by taking the branch cut along the negative imaginary E-axis so that in quadrants one through three we will use k in the physical upper-half plane and in quadrant four of the E-plane we will take k from the unphysical half-plane.

3 Relation of the poles and zeros of the single-channel S-matrix to quantum defect theory

There are important examples in dissociative electron attachment, like attachment to O_2^+ via the $^1\Sigma_u^+$ resonance, that can be treated with single-channel quantum defect theory. For that
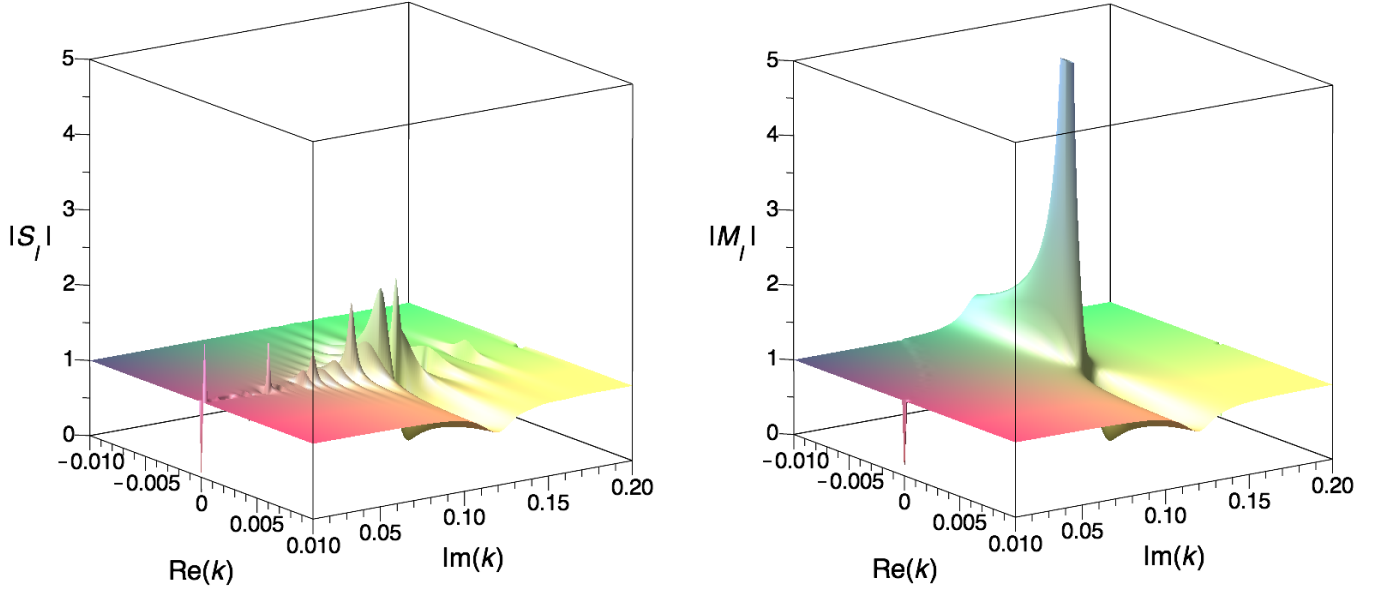
5

Figure 6: Plots of $|S_l^{\mathrm{SR}}|$ (left panel) and $|M_l|$ in the complex k-plane for the one channel model described in Eqs. (2) and (4) with $l = 4$, $Z = -1$, $r_0 = 3$, and $V_0 = 2.2$. The plotted $|M_l|$ has been smoothed in the region of the complex k-plane where $|Q|$ is growing exponentially, as indicated in Fig. 5.

reason, and to develop the general ideas that we will apply to the multichannel case, we turn now to the formal connection between the poles of the S-matrix and the quantum defects for a single channel problem. Once we have established that connection and developed a compact and accurate parametrization of it in terms of the motion of the poles and zeros of the S-matrix, we can turn to its application to the case of electron attachment to the O_2^+ ion. The result, presented in Section 3.4 below, is a unified representation of the results of *ab initio* bound state and scattering calculations not previously achieved.

3.1 General single-channel expressions

The asymptotic form of the $f_l^{\pm}$ Coulomb functions given in Appendix A are

$$f_l^+(k, r) \;\;\rightarrow\;\; e^{+i\rho_{\mathrm{c}}} \tag{12}$$
$$f_l^-(k, r) \;\;\rightarrow\;\; e^{-i\rho_{\mathrm{c}}} \tag{13}$$

where $\rho_{\mathrm{c}} = kr - n \ln 2kr$. In this section, we will only consider the case where the scattering potential is spherically symmetric, so that the different partial waves are decoupled. Then we can write the asymptotic form of the scattering states in terms of the partial-wave S-matrix, S_l, as

$$\psi(k, r) \to \frac{i}{2} \left[e^{i\pi l/2} f_l^-(k, r) - S_l(k) e^{-i\pi l/2} f_l^+(k, r) \right]. \tag{14}$$

This can be equivalently written in tems of the quantum defect, $\mu_l(k)$, as pointed out in the clear analysis of Chernov *et al.*,[15]

$$\psi(k, r) \to \frac{(k/i)^{-(l+1)} \sin(2\pi l)}{\sin \pi (2l - \mu_l(k))}$$

$$\times \left[\frac{e^{-\frac{i\pi\nu}{2}}}{\Gamma(1 + l + \nu)} \frac{\sin \pi (\mu_l(k) - \nu - l)}{\sin \pi (-\nu - l)} f_l^-(k, r) \right.$$

$$\left. - e^{-i\pi(\nu + l - \mu_l(k))} \frac{e^{+\frac{i\pi\nu}{2}}}{\Gamma(1 + l - \nu)} f_l^+(k, r) \right] \tag{15}$$

with $\nu = iZ/k$. Now if we define the short-range S-matrix, S^{SR}, by

$$S_l(k) = S_l^{\mathrm{SR}}(k)e^{i2\eta_l(k)} \qquad (16)$$

so that, in terms of the short range scattering phase shift, we have

$$S_l^{\mathrm{SR}}(k) = e^{i2\delta_l(k)}. \qquad (17)$$

The short-range S-matrix can be written in terms of the quantum defect as

$$S^{\mathrm{SR}}(k) = \frac{e^{i\pi\mu}\sin\pi(\nu + l)}{\sin\pi(\nu + l - \mu)}. \qquad (18)$$

On the positive imaginary k-axis, where ν and μ are real numbers, this clearly leads to zeros in S^{SR} at the hydrogenic energies, i.e $\nu + l = p$ where p is an integer, and poles at the bound states, i.e. where $\nu + l - \mu = p$. Now, by analogy to the relationship between the scattering phase-shift $\delta_l(k)$ which is related to the short-range S-matrix, we can define an M-matrix related to the quantum defect by

$$M_l(k) = e^{i2\pi\mu_l(k)}. \qquad (19)$$

Then the relationship between the S^{SR} and M is given by

$$\frac{1}{M_l(k)} = \frac{1}{S_l^{\mathrm{SR}}(k)}[1 - Q] + Q, \qquad (20)$$

where

$$Q = e^{\frac{2\pi Z}{k}}. \qquad (21)$$

or in terms of quantum defects and short-range scattering phase shifts we have

$$e^{-i2\pi\mu_l(k)} = e^{-i2\delta_l(k)}[1 - Q] + Q. \qquad (22)$$

Note that Eq. (22) is identical to Eq. (33) in the paper by Chernov et $al.$[15]

While $S_l^{\mathrm{SR}}(k)$ has both poles and zeros on the positive imaginary k-axis, the analytic structure of $M_l(k)$ is much simpler there. The central idea of quantum defect theory is to construct quantities determined entirely by the S-matrix for which a more straight-forward and functionally smooth connection can be made between real energies corresponding to the bound region

(positive imaginary k) and real energies in the continuum (positive real k). Here we examine the analytic continuation of such expressions to the entirety of the complex k-plane, which exposes their connection to the poles of the S-matrix and provides a parametrization in terms of them.

From Eq.(22) we can easily see that $M \approx S^{\mathrm{SR}}$ when $|Q| << 1$ or $\mathrm{Re}(-2\pi Z/k) >> 1$. In Fig. 5 we show $|Q|$ in both the k and E planes which indicate the range of momenta and energies over which one can approximate S^{SR} by M. We also indicate the region of the k and E planes where Q is growing exponentially. In that region, Eq. (20) cannot be evaluated accurately using finite precision arithmetic since when Q is large the value of M_l depends on the difference between S_l and 1, which is a small number on the order of $1/|Q|$. Also when $S_l^{\mathrm{SR}} = 0$ we have $M_l = 0$ except at the hydrogenic energies where $2\pi Z/k = ip2\pi$. Note that the zeros in S_l^{SR} at positive imaginary value of k are introduced in the transformation from the full S matrix as given in Eq. (16) and are not present in S_l whereas the poles in S_l^{SR} and S_l are at the same values of k. It is also clear from this equation that

$$\lim_{k\to 0^+}\exp\left(-2i\delta_l(k)\right) = \lim_{\kappa\to 0^+}\exp\left(-2i\pi\mu_l(i\kappa)\right) \qquad (23)$$

when $Z < 0$, which is the well-known result from Seaton.[23]

3.2 Parameterization of resonances with the single-channel quantum defect M_l

In the presence of a narrow resonance, the usual approach to characterizing the S_l^{SR} matrix in the region of a resonance is using a single-pole single-zero form[2]

$$S_l^{\mathrm{SR}} \approx e^{2i\delta_{\mathrm{bg}}}\frac{k - k_{\mathrm{res}}^*}{k - k_{\mathrm{res}}} \qquad (24)$$

where δ_{bg} is the background phase shift and k_{res} is the complex momentum at the location of the pole in S_l^{SR}. This approximation enforces the unitarity on S_l^{SR} for real values of k. Note that

in this form there is a corresponding zero in S_l^{SR} at k_{res}^*. In a similar fashion we can parameterize M_l using

$$M_l(k) \approx e^{2i\pi\mu_{\text{bg}}} \frac{(k - k_{\text{res}}^*)\,(k + k_{\text{res}}^*)}{(k - k_{\text{res}})\,(k + k_{\text{res}})}. \quad (25)$$

This approximation to M_l enforces unitarity for both purely real and purely imaginary values of k. The unitarity of M_l for purely imaginary values of k guarantees that the quantum defect will be real as needed for bound states to occur at real energies. The unitarity of S_l^{SR} at real values of k guarantees that M_l will be unitary when the real part of k is not too large. This expression for M_l can be rewritten in terms of energy to give

$$M_l(E) \approx e^{2i\pi\mu_{\text{bg}}} \frac{E - E_{\text{res}}^*}{E - E_{\text{res}}}. \quad (26)$$

Then the scattering phase shift or quantum defect at real energy can be extracted using the usual Breit-Wigner form[24]

$$\pi\mu_l(E) = \pi\mu_{\text{bg}} + \tan^{-1} \frac{\Gamma}{2\left[\text{Re}(E_{\text{res}}) - E\right]} \quad (27)$$

where $\Gamma = -2\,\text{Im}(E_{\text{res}})$.

3.3 Simple one-channel square-well model

We have computed the M_l function using Eq. (20) for the one-channel model described in Sec. 2 by Eqs. (2) and (4) with $l = 4$, $Z = -1$, $r_0 = 3$, and V_0 varying from 2.15 to 2.21. In Fig. 6 we show the absolute value of S_l and M_l in the upper half of the complex k-plane with $V_0 = 2.20$. We can see that, along the positive $\text{Im}(k)$ axis, S_l^{SR} has a series of poles and zeros which correspond to the poles of the actual Rydberg states and the zeros at the hydrogenic energies caused by the $\Gamma(l+1-in)$ function in the denominator of Eq. (3), as discussed above. M_l, in contrast to S_l, is a smooth function with only one zero in the first quadrant of the complex k-plane, with $k = 0.001778 + i0.1198$ or, in terms of the energy, at $E = -0.007171 + i0.0001065$ and a corresponding pole in the second quad-
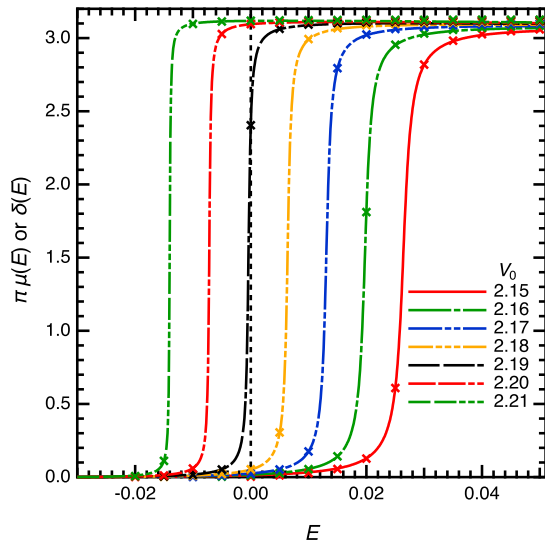

Figure 7: Scattering phase, $\delta(E)$ and quantum defects, $\pi\mu(E)$ computed using $\arg(M)/2$ for the square well + Coulomb model given in Eqs. (2) and (4) with $l = 4$, $Z = -1$, $r_0 = 3$ for different strengths with $V_0 = 2.15$ to 2.21 for real energies. The simple one-pole-one-zero approximation obtained using Eq. (25) and an energy independent background phase shift are indicated with the crosses. The value k_{res}^* used for each potential strength was that obtained by finding the zeros of M_l in the first quadrant of the complex k-plane. Note the S_l^{SR} has the same zeros as M_l.

rant of the complex k-plane. As seen in Fig. 3, the real part of the energy of this zero, also found in S_l^{SR}, will move to higher energy as the value of V_0 is decreased.

In Fig. 7, we plot the quantum defects and scattering phases computed from M_l for this problem for a series of potential strengths. We can see that for this model, the width of the resonance increases as the potential is made weaker. Additionally, we plot the results of using Eq. (25) to model the behavior of M_l at real energies. The values of k_{res} used in the expression were those shown in Fig. 3, which were obtained by solving for the zeros and poles of S_l and M_l as a function of V_0. Additionally, a small energy-independent background phase was added to obtain a good fit. This result shows that Eq. (25) provides a good description of how the poles and zeros in S_l and M_l determine the behavior of the eigenphases and quantum defects at real energies. This also suggests that Eq. (25) could be used to take scattering phases and quantum defects at real energies an infer the location of the resonance poles and zeros.

It is instructive to note that the behavior of the poles and zeros of the one-channel M-matrix in the complex k-plane is similar to the behavior of the poles and zeros of an S-matrix in multichannel scattering with short-range potentials as described by Newton[25] where a k-plane diagram appears similar to the lower half of Fig. 3. While that subject is in general quite complicated, we can see an analogy with the single-channel Coulomb scattering case by considering a three channel case with only short-range potentials and three different thresholds, $E_1 < E_2 < E_3$ in the context of Newton's analysis. Assume that there is a resonance caused by a nearly bound state in channel 3 but through coupling to the open channels 1 and 2 has a finite lifetime such that a pole in the S matrix occurs between the second and third thresholds at E_{res} and that $E_2 < \mathrm{Re}(E_{\mathrm{res}}) < E_3$ and $\mathrm{Im}(E_{\mathrm{res}}) < 0$. In that case, the position of the resonance will be described with k_1 and k_2 being on the unphysical lower half of the complex k-plane, i.e. with $\mathrm{Im}(k_1) < 0$ and $\mathrm{Im}(k_2) < 0$, while k_3 is on the physical upper half plane with $\mathrm{Im}(k_3) > 0$. Now if the potential is made more attractive without shifting the thresholds, the energy of the resonant state can be lowered so that $E_1 < \mathrm{Re}(E_{\mathrm{res}}) < E_2$ so that the resonance lies between the first two thresholds. Now the only open channel is channel 1. The pole that corresponds to this resonance will then have $\mathrm{Im}(k_1) < 0$ but both $\mathrm{Im}(k_2) > 0$ and $\mathrm{Im}(k_3) > 0$. The width of the resonance does not go through zero as channel 2 is closed so that the trajectory of the pole in the k_2-plane cannot go through the origin. Thus the pole in the complex k_2-plane when channel 2 is closed does not connect to the pole in the k_2-plane when channel 2 is open.

In a similar fashion for the Coulomb plus short range problem, the width of the resonant state, which causes the pole in the M-matrix, does not go to zero as the energy of the resonance goes below the last threshold. Thus the trajectory of the pole in the complex k-plane cannot go through the origin. However there is a new pole in the M matrix which appears in the second quadrant, i.e. the physical part of the of the complex k-plane which then moves close to the positive imaginary k-axis as the short range potential becomes more attractive. Note that this behavior is only seen in the M-matrix and not in S^{SR}.

3.4 One-channel treatment of e-O_2^+ scattering

Here we apply the one-channel M-matrix analysis of Section 3.1 to the $^1\Sigma_u^+$ resonance in e-O_2^+ scattering. The direct dissociative recombination in e-O_2^+ scattering is believed to be proceed through a doubly-excited (Feshbach) resonance of $^1\Sigma_u^+$ symmetry which is formed in the collision of a low-energy electron with the O_2^+ molecule in its $X^2\Pi_g$ ground state.[4] The main electronic configuration in the ion is $\ldots 3\sigma_g^2 1\pi_u^4 1\pi_g$ while that of the resonant $^1\Sigma_u^+$ state is $\ldots 3\sigma_g^2 1\pi_u^3 1\pi_g^3$.[26] In this case we can use the parametrization of Section 3.2 to extract the trajectory of the pole and zero in the S-matrix, and the corresponding M-matrix, to illustrate how the scattering resonance is converted into a pole and zero combination in the
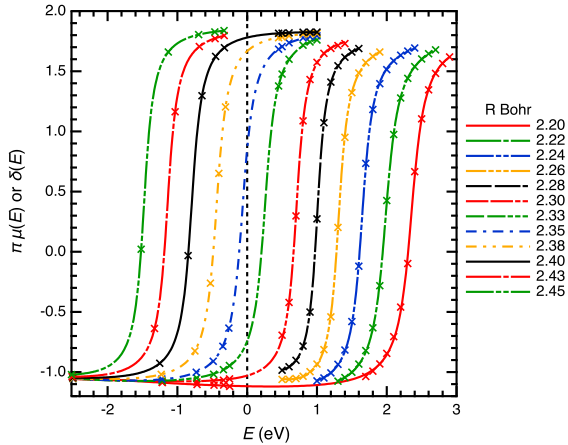
Figure 8: Computed quantum defects and scattering phase shifts for the $l = 1$ one-electron continuum functions in the e-O_2^+ system with total symmetry of $^1\Sigma_u^+$. The lines are the one-pole-one zero model fits using Eq. (27) compared to computed quantum defects and phases for the geometries ranging from $R_{O\text{-}O} = 2.2$ Bohr to 2.45 Bohr.

M-matrix below threshold. This structure in the M-matrix causes a resonance structure in the quantum defect which is reflected in shifts in the Rydberg energies as a function of molecular geometry.

Both the scattering and the bound state calculations of this process were performed with a one-electron basis that contained a triple-zeta with polarization basis on the oxygen atoms[27] plus 16 additional p functions at the bond center, chosen with exponents in a geometric series ranging from $\alpha = 0.12$ to 0.000056. The molecular orbitals were obtained from a multi-configuration self consistent field calculation on O_2^+ ($^2\Pi_g$). Ten target orbitals were included: three σ_g, three σ_u, one π_{ux}, one π_{uy}, one π_{gx} and one π_{gy}. The MCSCF wave function only contained configurations in which the three σ_g and two of the σ_u orbitals were doubly occupied. The bound Rydberg and scattering states of overall $^1\Sigma_u^+$ symmetry were then constructed by doubly occupying the first five ion orbitals and allowing the remaining six electrons to occupy the remaining active and virtual orbitals, with the restriction that no more than one electron occupy a virtual orbital. The scattering calculations were performed using the complex

Kohn method.[28]

In Fig. 8 we plot the $l = 1$ partial-wave scattering phases and quantum defects from $l = 1$ Rydberg state energies of $^1\Sigma_u^+$ symmetry near the resonance in e-O_2^+ on a grid of geometries with $R_{O\text{-}O} = 2.2$ Bohr to 2.45 Bohr. The lines presented there are Breit-Wigner forms given in Eq. (27) that have been fit to the computed data. The results for each geometry were fit separately with the background scattering represented as a quadratic function of E. The resulting real parts of the resonance energies relative to the ionization potential of O_2 and the widths are plotted as a function of R in Fig. 9. The results are compared to the computed results of Guberman and Giusti-Suzor.[4] We see that the position of our computed resonances are at a slightly higher energy for a given geometry and our computed widths are close to those obtained by Guberman and Giusti-Suzor. However, in the present calculations we see that there is some structure near the geometry where resonance is at threshold, which however is not fully resolved here. These extracted energy parameters are replotted as trajectories of zeros and poles in the complex k-plane in Fig. 10. The zero and pole trajectories found here are very close to those extracted from the previously published data. The results presented here indicate that we have achieved a combined bound state and scattering calculation unlike any previous study.

4 Relation of the poles and zeros of the multichannel S-matrix to quantum defect theory

With the analysis of the analytic structure of single-channel quantum defect theory in the complex momentum and energy planes in hand, we proceed to apply the same ideas to the multichannel case. The resulting working equations depart from the traditional formulation of multichannel quantum defect theory, and, while being functionally equivalent for real values of the energy, they expose the connection to the mo-
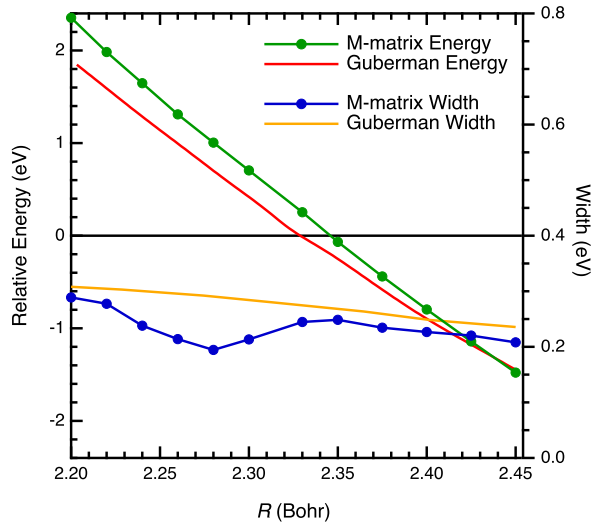
10

Figure 9: Resonance energies and widths for the $^1\Sigma_u^+$ resonance in the $e\text{-}O_2^+$ system. The present results are compared to the computed results of Guberman and Giusti-Suzor.[4]

tion of the poles and zeros of the multichannel S-matrix. Dissociative electron attachment to the H_2^+ ion via the $^1\Sigma_g$ resonance that is dominated by the $1\sigma_u^2$ configuration can be treated as a three-channel problem. Application of this formulation in Section 4.4 below allows us to construct a unified description of *ab initio* electronic structure and scattering calculations that reveals the motion of the relevant pole and zero of the S-matrix.

4.1 Multichannel expressions

The single-channel expressions given in the preceding section can be generalized to the case of multiple coupled channels where the additional coupled channels can correspond to different asymptotic angular momenta of the Rydberg or scattered electrons with the same core electronic state or with different core electronic states. First we define energy-normalized $\mathcal{F}_i^{\pm}$ functions which are closely related to the $f_l^{\pm}$ functions used in the previous section but are now indexed by the channel, i,

$$\mathcal{F}_i^+(\vec{r}) = \left(\frac{2}{\pi k_i}\right)^{\frac{1}{2}} e^{-i\frac{\pi}{2}l_i} e^{i\eta_{l_i}(k_i)} f_{l_i}^+(k_i, r) Y_{l_i m_i}(\hat{r})$$
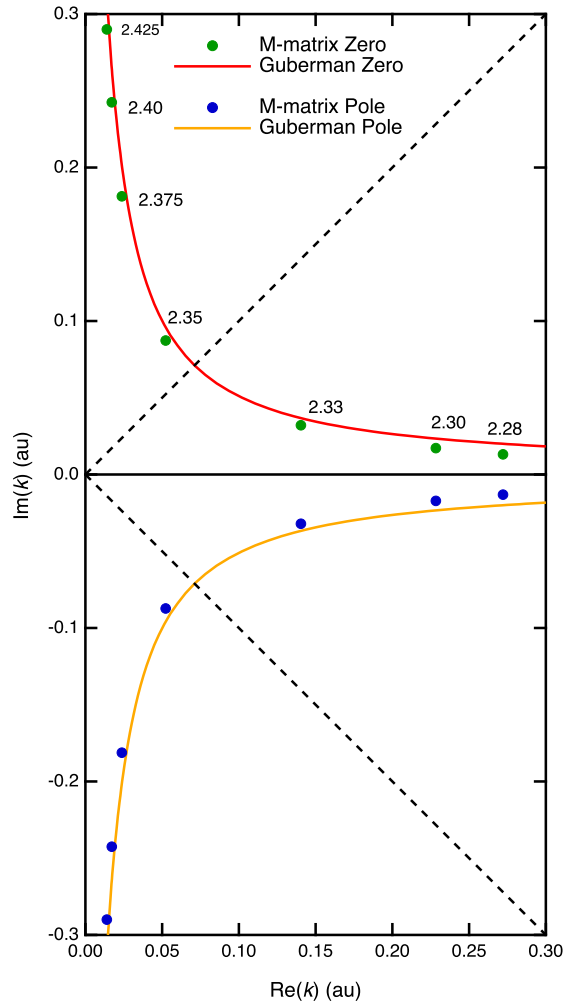
$$(28)$$

Figure 10: Trajectories of the zeros and poles of the M-matrix for the $^1\Sigma_u^+$ resonance in the $e\text{-}O_2^+$ system. The value of R in Bohr at selected points is indicated on the graph. The present results are compared to zero and pole trajectories extracted from the computed results of Guberman and Giusti-Suzor.[4]

$$\mathcal{F}_i^-(\vec{r}) = \left(\frac{2}{\pi k_i}\right)^{\frac{1}{2}} e^{i\frac{\pi}{2}l_i} e^{-i\eta_{l_i}(k_i)} f_{l_i}^-(k_i, r) Y_{l_i m_i}(\hat{r}),$$

$$(29)$$

where $k_i = \sqrt{2(E - E_i)}$ is the asymptotic momentum in channel i, E_i is the threshold for channel i, and (l_i, m_i) are the asymptotic angular momentum quantum numbers of the electron in channel i. Using these functions, the asymptotic form of the multichannel partial-wave scattering state, $\psi_j^S(\vec{r})$, can be written in terms of the short-range S^{SR}-matrix, and will

have the form

$$\psi_j^S(\vec{r}) \rightarrow \sum_i \frac{i}{2} \left[\mathcal{F}_i^-(\vec{r})\delta_{i,j} - \mathcal{F}_i^+(\vec{r})S_{i,j}^{\mathrm{SR}} \right]. \quad (30)$$

where j is the index of the channel containing the homogeneous solution of the Schrodinger equation.

To construct a multichannel quantum-defect matrix we define an alternative pair of linearly independent Coulomb functions

$$\begin{aligned} \tilde{\mathcal{F}}_i^+(\vec{r}) &= \mathcal{F}_i^+(\vec{r})(1 - \tilde{Q}_i)^{\frac{1}{2}} \\ &\quad + \mathcal{F}_i^-(\vec{r})\tilde{Q}_i(1 - \tilde{Q}_i)^{-\frac{1}{2}} \quad (31) \\ \tilde{\mathcal{F}}_i^-(\vec{r}) &= \mathcal{F}_i^-(\vec{r})(1 - \tilde{Q}_i)^{-\frac{1}{2}}, \quad (32) \end{aligned}$$

where, for real energies, $\tilde{Q}_i$ is defined as

$$\tilde{Q}_i = \begin{cases} 0 & E > E_i \\ e^{-i2\pi(\nu_i + l_i)} & E < E_i \end{cases}, \quad (33)$$

where, as in the one channel case, $\nu_i = iZ/k_i$. We can now define the multi-channel version of the quantum defect M-matrix in terms of the asymptotic form of the wave function using

$$\psi_j^M(\vec{r}) \rightarrow \sum_i \frac{i}{2} \left[\tilde{\mathcal{F}}_i^-(\vec{r})\delta_{i,j} - \tilde{\mathcal{F}}_i^+(\vec{r})M_{i,j} \right]. \quad (34)$$

Matching asymptotic forms given in Eq. (30), we can see that the relationship between $\mathbf{S}^{\mathrm{SR}}$ and $\tilde{\mathbf{M}}$ is

$$\left(\mathbf{S}^{\mathrm{SR}}\right)^{-1} = \left(\mathbf{1} - \tilde{\mathbf{Q}}\right)^{-\frac{1}{2}} \left(\tilde{\mathbf{M}}^{-1} - 1\right) \left(\mathbf{1} - \tilde{\mathbf{Q}}\right)^{-\frac{1}{2}} + 1 \quad (35)$$

where the $\tilde{\mathbf{Q}}$ matrices are diagonal, with elements given above, i.e. $\tilde{\mathbf{Q}}_{i,j} = \delta_{i,j}\tilde{Q}_i$. Note that the square-root terms in Eq. (35), $\left(\mathbf{1} - \tilde{\mathbf{Q}}\right)^{-\frac{1}{2}}$, do not introduce any sign ambiguity as long as both such factors take the same branch of the square-root function. The relationship can be inverted to give

$$\tilde{\mathbf{M}}^{-1} = \left(\mathbf{1} - \tilde{\mathbf{Q}}\right)^{\frac{1}{2}} \left(\mathbf{S}^{\mathrm{SR}}\right)^{-1} \left(\mathbf{1} - \tilde{\mathbf{Q}}\right)^{\frac{1}{2}} + \tilde{\mathbf{Q}}. \quad (36)$$

By construction, we see that the complex symmetric $\mathbf{S}^{\mathrm{SR}}$-matrix will always lead to a complex symmetric $\tilde{\mathbf{M}}$-matrix.

In general, when all channels are closed, the condition for a bound state is that asymptotically the wave function only contains exponentially decaying radial functions. On the physical upper-half of the complex k-plane, i.e. where $\mathrm{Im}(k_i) \geq 0$, bound states occur at real energies when the wave functions do not contain any asymptotic contribution from the $\mathcal{F}^-$ functions, which are exponentially growing. From Eq. (30), we can see that bound states will then occur when $\det\left[\left(\mathbf{S}^{\mathrm{SR}}\right)^{-1}\right] = 0$. Similarly, in terms of the $\tilde{\mathbf{M}}$-matrix, the bound states will occur when

$$\det\left(\mathbf{1} - \tilde{\mathbf{Q}}\tilde{\mathbf{M}}\right) = 0. \quad (37)$$

In addition to the solutions of Eq. (37) which occur at the correct bound states, there are also solutions which occur at unphysical hydrogenic energies in each channel, i.e. where

$$E - E_i = -\frac{1}{2n^2}, \quad (38)$$

where n is an integer and $n \leq l_i$. These occur because of the definition of Q which causes $Q_i = 1$ both at the energy of true hydrogenic energies and at the unphysical energies where $n \leq l_i$. At the energies of the true hydrogenic states, the corresponding zeros on the diagonals of $\mathbf{1} - \tilde{\mathbf{Q}}$ just cancel out the zeros that occur in $\mathbf{S}^{\mathrm{SR}}$. Then at the unphysical hydrogenic energies $(n \leq l_i)$ this definition of Q leads to unphysical solutions of Eq. (37). The unphysical solutions of Eq. (37) can be avoided by searching for solutions of the modified equation

$$0 = \frac{\det\left(\mathbf{1} - \tilde{\mathbf{Q}}\tilde{\mathbf{M}}\right)}{\prod_{i=1}^{N} z_i^2} \quad (39)$$

where

$$z_i(E) = \left[\prod_{n_i=1}^{l_i} \left(E - E_i + \frac{1}{2n_i^2} \right) \right]^{\frac{1}{2}}. \quad (40)$$

If all channels are open, then we have $\tilde{\mathbf{Q}} = 0$ so that from Eq. (36) we see that $\tilde{\mathbf{M}} = \mathbf{S}^{\mathrm{SR}}$

The definition of $\tilde{Q}_i$ given in Eq. (33) is only

appropriate at real energies. However the objective of the present study is to consider the analytic continuation of the $\mathbf{S}$ matrix into the complex E-plane near channel thresholds. For this purpose we define a modified $\mathbf{Q}$ with diagonal elements given by

$$Q_i = e^{-i2\pi(\nu_i + l_i)} \text{ for all channels } i. \qquad (41)$$

Then we can define an alternate quantum defect matrix $\mathbf{M}$, in analogy to Eq. (36), as

$$\mathbf{M}^{-1} = (\mathbf{1} - \mathbf{Q})^{\frac{1}{2}} \left(\mathbf{S}^{\mathrm{SR}}\right)^{-1} (\mathbf{1} - \mathbf{Q})^{\frac{1}{2}} + \mathbf{Q}, \ (42)$$

where the inverse relationship between $\mathbf{M}$ and $\mathbf{S}^{\mathrm{SR}}$ is

$$\left(\mathbf{S}^{\mathrm{SR}}\right)^{-1} = (\mathbf{1} - \mathbf{Q})^{-\frac{1}{2}} \left(\mathbf{M}^{-1} - 1\right) (\mathbf{1} - \mathbf{Q})^{-\frac{1}{2}} + 1 \tag{43}$$

which is obtained from Eq. (35) by removing the tildes. Note that, when there is only one channel, $\mathbf{M}$ is the same as M_l given in Eq. (20). If all of the channels are closed, the definition of $\mathbf{Q}$ is exactly the same at real energies as $\tilde{\mathbf{Q}}$ from Eq. (33) so that at real energies $\mathbf{M} = \tilde{\mathbf{M}}$. Then the condition for the bound states found in Eq. (39) can be rewritten as

$$0 = \frac{\det\left(\mathbf{1} - \mathbf{QM}\right)}{\prod_{i=1}^N z_i^2}. \tag{44}$$

Furthermore, if any of the channels are open and the open-channel momenta satisfy $\mathrm{Re}(-2\pi Z/k_i) >> 1$ we have $\mathbf{M} \approx \tilde{\mathbf{M}}$. In general, if an open channel momentum has a large positive real part one can take $Q_i = 0$ for that channel as long as one does not try to extend the analysis to energies where that channel becomes closed.

4.2 Parameterization of the multichannel quantum defect M

The $\mathbf{M}$-matrix has many properties of a scattering $\mathbf{S}^{\mathrm{SR}}$ matrix. It is complex symmetric, and at real energies its eigenvalues have unit norm. Thus we can parameterize $\mathbf{M}$ using a real-symmetric $\mathbf{K}$-matrix where

$$\mathbf{M} = (\mathbf{1} + i\tilde{\mathbf{K}})(\mathbf{1} - i\tilde{\mathbf{K}})^{-1} \tag{45}$$

where we have explicitly included the source of the unphysical roots found in Eq. (37) using

$$\tilde{K}_{i,j} = z_i z_j K_{i,j} \tag{46}$$

where, for real energies, $\mathbf{K}$ is a real symmetric matrix that varies slowly with energy.

In general for a system where a set of quantum defects and scattering matrices have been computed, we will then want to extract the values of the $\mathbf{K}$ matrix by fitting the computed data. For the bound part of the spectrum we can fit the solutions of Eq. (44) for assumed values of $\mathbf{K}$ and for purely open channel energies we can extract the $K_{i,j}$ using $\mathbf{M} \approx \mathbf{S}^{\mathrm{SR}}$. To extract the values of the $K_{i,j}$ when there are both open and closed channels, one can still use Eqs. (43), (45), and (46) to obtain a model $\mathbf{S}^{\mathrm{SR}}$ matrix from the assumed values of $\mathbf{K}$. Then only the resulting open-channel $\mathbf{S}_o^{\mathrm{SR}}$ should be fit to scattering data. Computing the $\mathbf{S}_o^{\mathrm{SR}}$ from the full $\mathbf{M}$ matrix is the same as "elimination" of the closed channels found in the standard K-matrix quantum defect theory.[29]

4.3 The M-matrix for a simple three-channel model

To illustrate the multi-channel version of the M-matrix theory of quantum defects we will first consider an exactly-solvable simple model constructed from square-wells where the coupled-channel Schrodinger is

$$-\frac{1}{2}\frac{d^2\psi_i(r)}{dr^2} + \sum_j V_{i,j}\psi_j(r) = E\psi_i(r) \qquad (47)$$

and using a potential of the form

$$V_{i,j}(r) = \begin{cases} V_{i,j}^{\mathrm{SR}} & r \le r_0 \\ \delta_{i,j}\left[\frac{Z}{r} + \frac{l_i(l_i+1)}{2r^2} + E_i\right] & r > r_0 \end{cases}, \tag{48}$$

where in this study we will take $l_1 = 0$, $l_2 = 2$, $l_3 = 1$, $Z = -1$, $E_1 = E_2 = 0$, $E_3 = 0.7$, and $r_0 = 3$. The short-range potential was parameterized with $V_{1,1}^{\mathrm{SR}} = -0.6$, $V_{1,2}^{\mathrm{SR}} = V_{2,1}^{\mathrm{SR}} = 0$, $V_{1,3}^{\mathrm{SR}} = V_{3,1}^{\mathrm{SR}} = 0.2, V_{2,2}^{\mathrm{SR}} = 0.35$ with $V_{3,3}^{\mathrm{SR}}$ being varied, with a typical vallue being -0.7. In this model, all three channels are closed with

$E < 0$, the $l = 0$ and $l = 2$ channels are open and the $l = 1$ channel is closed for $0 < E < 0.7$. For a range of $V_{3,3}$ values there is a resonance which occurs for just above $E > 0$ in addition to the Rydberg resonances which occur just below the last threshold at $E_3 = 0.7$. As $V_{3,3}$ becomes more negative the lowest resonance from the $l = 1$ channel moves below $E = 0$ and perturbs the Rydberg states in the other two channels. This model is similar to the e-H_2^+ problem considered below in Sec. 4.4 with the same number of channels and the same asymptotic partial waves and with variations in $V_{3,3}$ shifting the energy of the resonance in analogy to changing the bond length in the molecular case.

With a multi-channel S-matrix, the behavior of individual matrix elements does not generally provide a basis for the analysis of the bound states and resonances. Instead we will use $\det(\mathbf{S}^{SR})$ and $\det(\mathbf{M})$. First, in Fig. 11 we show the three-dimensional plots of $\left| \det\left(\mathbf{S}^{SR}\right) \right|$ and $\left| \det\left(\mathbf{M}\right) \right|$ in the energy plane for $V_{3,3} = -0.7$. In these calculations we have chosen the branch-cut in the complex energy plane to be on the negative imaginary energy axis, as indicated in the lower panel of Fig. 5. With this choice, the $\mathbf{S}$ and $\mathbf{M}$ functions smoothly connect in the region of the real energy axis but can have discontinuities across the negative imaginary energy axis. We can see that $\left| \det\left(\mathbf{S}^{SR}\right) \right|$, which uses the full 3×3 matrix including both open and closed channels, contains a pole at an energy above zero but below E_3. Additionally, the $\left| \det\left(\mathbf{S}_o^{SR}\right) \right|$ determined from the 2×2 open channel sub-matrix has the same pole structure and additionally there is a corresponding zero in the first quadrant of the complex E-plane. Note that with closed channels, $\mathbf{S}^{SR}$ is no longer unitary at real energies. However, at positive real energies with $0 < E < 0.7$ the open channel $\mathbf{S}_o^{SR}$ is unitary so that a pole at $E_{res} - i\Gamma/2$ must be paired with a zero at $E_{res} + i\Gamma/2$, as seen in the lower-left panel of Fig. 11.

On the right hand side of Fig. 11 we show the corresponding plots for $\left| \det\left(\mathbf{M}\right) \right|$ and $\left| \det\left(\mathbf{M}_o\right) \right|$, obtained from Eq. (42) with $\mathbf{S}_o^{SR}$ replacing $\mathbf{S}^{SR}$. $\left| \det\left(\mathbf{M}\right) \right|$ has no structure and is smoothly varying over the range of energies presented. This is what one would expect from a quantum-defect treatment where all of the structure due to interactions with closed channels has been removed with the transformation given in Eq. (42). In the lower right panel of the figure we show $\left| \det\left(\mathbf{M}_o\right) \right|$ which is computed from the open channel S-matrix. We can see here that, above the threshold for the open channels at $E = 0$, $\left| \det\left(\mathbf{M}_o\right) \right|$ is the same as $\left| \det\left(\mathbf{S}_o^{SR}\right) \right|$. Then below that energy, the poles and zeros have been removed in the M-matrix. Thus the three-channel problem can be analyzed using $\mathbf{M}$ in which all of the resonances and bound states due to the interaction of Rydberg states found in $\mathbf{S}^{SR}$ have been removed in the transformation to $\mathbf{M}$. Alternatively, the isolated resonance in the third channel above the $E = 0$ threshold can be treated using $\mathbf{M}_o$ where the resonance will appear as a pole-zero combination which will then move as a function of the parameters of the problem. The fact that $\mathbf{M}_o$ contains the zero and pole structure coming from an isolated closed-channel resonance is the reason that we could successfully model the e-O_2^+ resonance problem in Sec. 3.4, which is inherently at least a two channel problem with one open and one closed channel, as a one-channel problem.

Just as we did in the case of the single channel model considered in Sec. 3.3, we can follow the behavior of the prominent resonance seen in Fig. 11 as a function of the potential strength parameter $V_{3,3}$ using the $\mathbf{M}_o$ representation. In Fig. 12 we see the trajectory of the resonance in the complex k-plane, where k is the momentum in the two channels that have thresholds at $E = 0$. As in the one-channel case the trajectory of this isolated resonance does not pass through the origin but has the pole moving to larger negative imaginary parts of k as the zero moves towards larger positive imaginary k where it interacts with the Rydberg states below the $E = 0$ threshold. In Fig. 13 we plot the real part of the resonance energy and the width of the resonance as a function of $V_{3,3}$. We see that the real part of the resonance energy becomes negative at $V_{3,3} = -0.804$. The resonance width at the threshold of this Feshbach resonance is fairly broad but becomes narrower
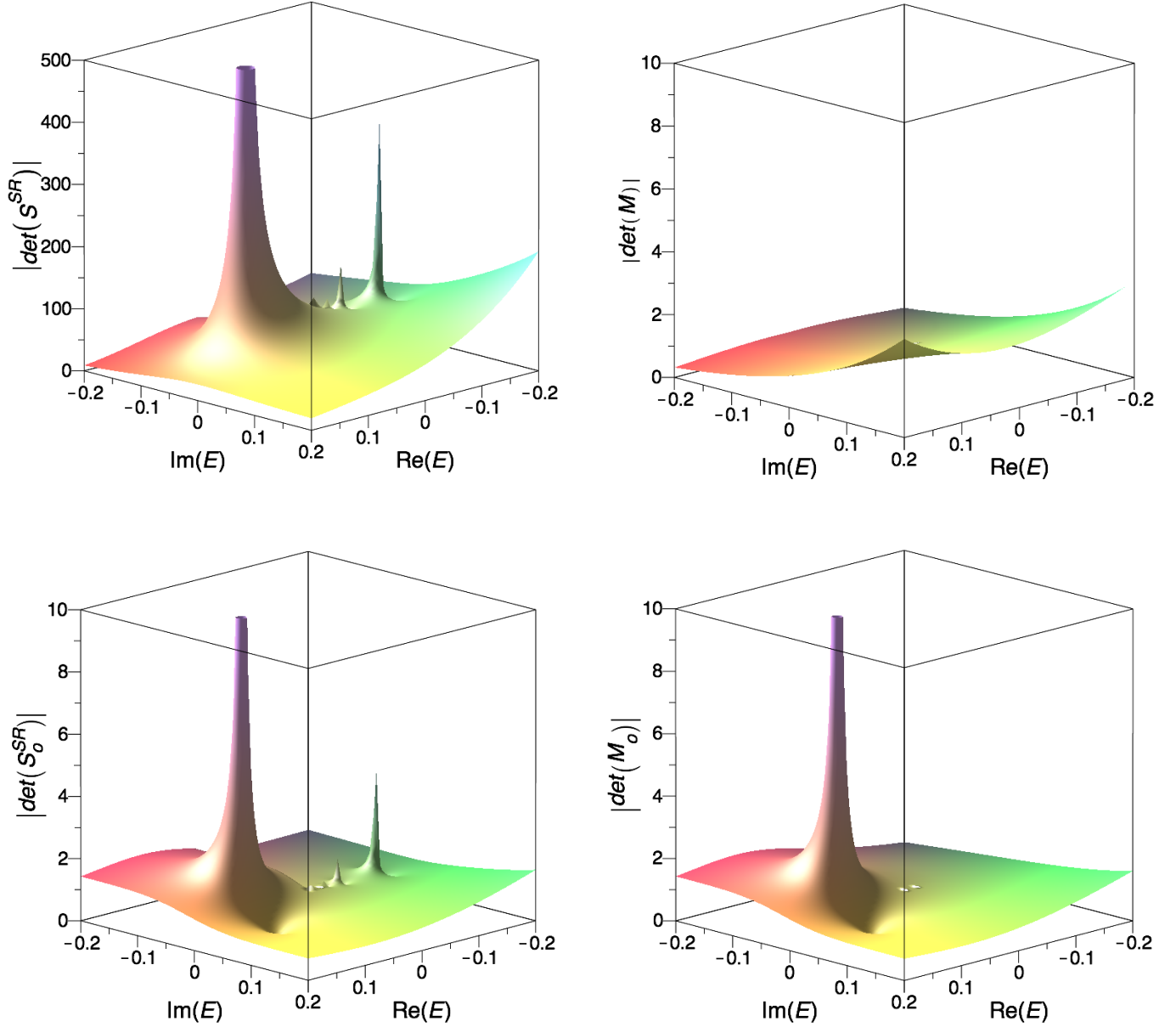
Figure 11: Plots of $|\det\left(\mathbf{S}^{\mathrm{SR}}\right)|$ (upper left panel), $|\det\left(\mathbf{S}_o^{\mathrm{SR}}\right)|$ (lower left panel), $|\det\left(\mathbf{M}\right)|$ (upper right panel) and $|\det\left(\mathbf{M}_o\right)|$ (lower right panel) in the complex E-plane for the three-channel model described in Eqs. (48) and (47) with the parameters defined in the text and with $V_{3,3} = -0.7$. For both $|\det\left(\mathbf{M}\right)|$ and $|\det\left(\mathbf{M}_o\right)|$, in the region of the complex E-plane where $|Q|$ is growing exponentially, as indicated in Fig. (5), the plotted results have been interpolated from regions where the numerical calculations were stable.
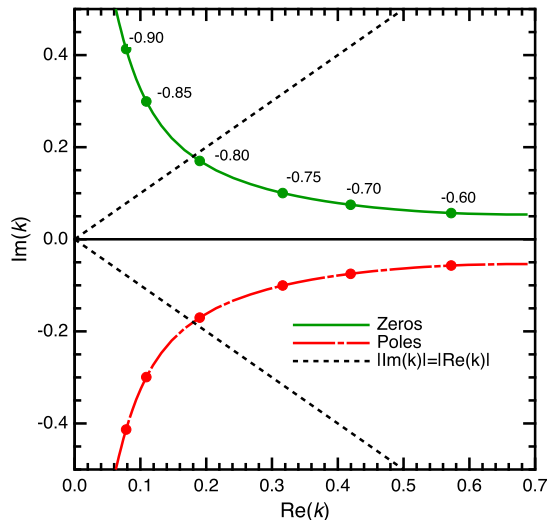
Figure 12: Trajectories of the zeros and poles of the three-channel model from $\mathbf{M}_o$ as a function of $V_{3,3}$.

Figure 13: Resonance energies and widths for the three-channel model from $\mathbf{M}_o$ as a function of $V_{3,3}$.

as the energy of the zero moves to more negative values with the value of $V_{3,3}$ becoming more negative.

4.4 Three-channel analysis of e-H_2^+ scattering

A molecular system that can be represented as a three-channel probelm is the resonance in $^1\Sigma_g^+$ symmetry in e-H_2^+ scattering.[30–32] This is the smallest molecular system which can exhibit Feshbach type resonances and can be accurately treated using *ab initio* methods. In this problem, both above and below the threshold for ionization of H_2, the $^1\Sigma_g^+$ resonance, which is dominated by the $1\sigma_u^2$ configuration, couples strongly with the $l = 0$ and $l = 2$ continua above the ionization threshold and the corresponding $l = 0$ and $l = 2$ Rydberg states below threshold. Thus the description of the $^1\Sigma_g^+$ resonance is dominated by the three channels with configurations $(1\sigma_g)(ks\sigma_g)$, $(1\sigma_g)(kd\sigma_g)$, and $(1\sigma_u)(kp\sigma_u)$.[32] At H_2 bond distances less than 2.7 Bohr the resonance appears in the scattering and at longer bond lengths the resonance appears as a perturbation of the ns and nd Rydberg series.

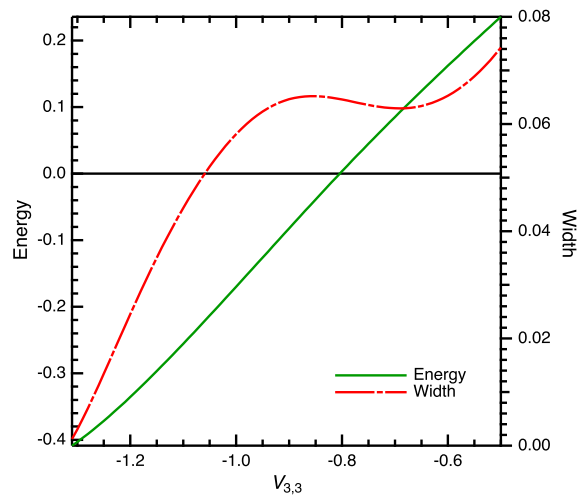In all bound states computed for this system we used a one-electron basis that con-

tained an aug-cc-pVTZ basis set on the hydrogen atoms[33,34] plus additional s, p, and d basis functions at the bond center, optimized to represent Rydberg states,[35] with nine functions with exponents ranging from $\alpha = 0.01125$ to 0.0003318 for $l = 0$, ten functions with exponents ranging from $\alpha = 0.06054$ to 0.0007901 for $l = 2$, and two diffuse $l = 1$ functions with $\alpha = 0.04234$ and 0.01925. The scattering was computed using a coupled channel representation of the wave function[36,37] with the targets being the lowest seven eigenstates of H_2^+ including three $^2\Sigma_g^+$ states, two $^2\Sigma_u^+$ states, one $^2\Pi_u$ state, and one $^2\Pi_g$ state. The bound state calculation of the Rydberg states of $^1\Sigma_g^+$ symmetry had up to two electrons in the seven target states and up to one electron in the virtual orbitals.

The scattering and bound states of $^1\Sigma_g^+$ symmetry were computed at a range of $R_{\text{H-H}}$ distances from 2.0 to 3.2 Bohr which spans the range of bond distance where the resonance transitions from being a scattering resonance to a perturbation of the Rydberg series. At each value of $R_{\text{H-H}}$ the scattering $\mathbf{S}_o^{\text{SR}}$ was computed for energies from the threshold for ionization leading to the ground state of H_2^+ up to 3.25 eV below the threshold leading to the $^2\Sigma_u^+$ ion state. Below the ionization threshold the s and d Rydberg series were computed up to $n = 6$.
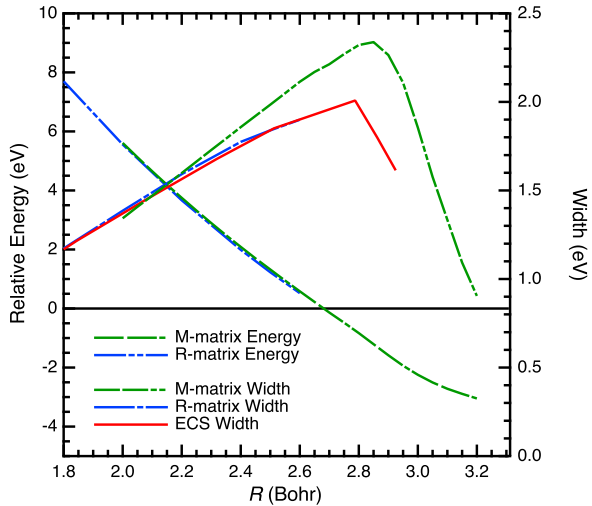
Figure 14: Energy and width of the $^1\Sigma_g^+$ resonant state of the e-H_2^+ system from $\mathbf{M}_o$ as a function $R_{\text{H-H}}$. R-matrix results are from Ref.[30] and the ECS results are from Ref.[31]

Although the computed $\mathbf{S}_o^{\text{SR}}$ at each $R_{\text{H-H}}$ could have been fit to a multichannel extension of the Breit-Wigner form[24,38] we found that, to parameterize both bound and continuum energies, fitting the 3×3 $\mathbf{K}$-matrix as defined in Eqs. (45) and (46) led to fewer parameters and a consistent treatment of the data. For each value of $R_{\text{H-H}}$, a 3×3 $\mathbf{K}$-matrix was fit using energy-independent values of $K_{1,2}$, $K_{2,2}$, $K_{3,3}$ and using $K_{1,1}$, $K_{1,3}$, $K_{2,3}$ which were assumed to depend linearly on E. For the scattering energies, the assumed $\mathbf{K}$-matrix was then used to compute $\mathbf{M}$ using Eqs. (45) and (46), which was then used to compute $\mathbf{S}^{\text{SR}}$ using Eq. (43) from which $\mathbf{S}_o^{\text{SR}}$ was extracted. Additionally, the positions of the bound states were found by solving Eq (44). The nine parameters used to define $\mathbf{K}$ at a given $R_{\text{H-H}}$ were optimized to obtain the best least-squares agreement between the computed and model $\mathbf{S}_o^{\text{SR}}$ and bound state energies.

In Fig. 14 we show the computed resonance positions and resonance widths as a function of $R_{\text{H-H}}$ and compare our values to previously published results for the energy of the scattering resonance[30] and the width.[30,31] Note that in Ref.[31] the width, estimated from an exterior complex scaling (ECS) calculation, is given for a geometry where the resonance has gone
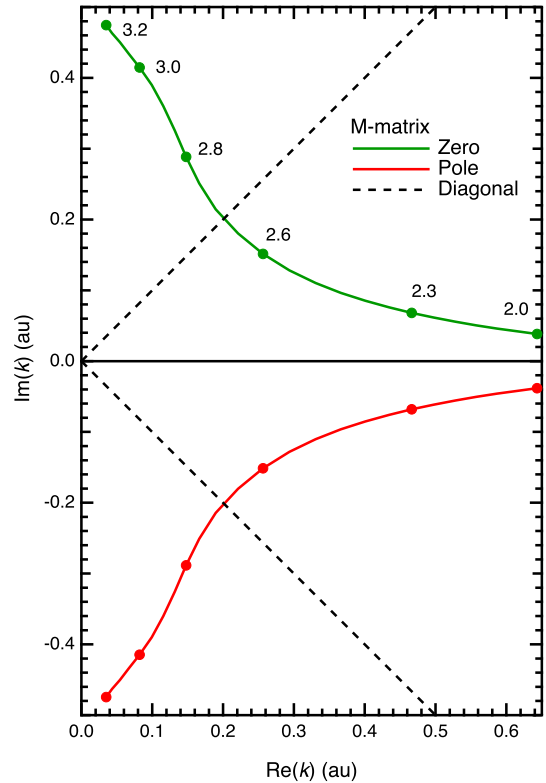

Figure 15: Trajectories of the zeros and poles of the $^1\Sigma_g^+$ resonant state of the $e-H_2^+$ system from $\mathbf{M}_o$ as a function of $R_{\text{H-H}}$. The value of R in Bohr at selected points is indicated on the graph.

below the threshold. The agreement between our computed resonance positions and those obtained from R-matrix scattering calculations is very good[30] although our computed widths between $R = 2.3$ and 2.6 Bohr increase linearly while those from the R-matrix calculations increase somewhat less rapidly. The qualitative behavior of widths from Ref.[31] is similar to what is found here, i.e. the total width rises as the bond get longer until the resonance goes below threshold at which point the width of the resonance becomes narrower. Our computed resonance widths and energies have been plotted in Fig. 15 as the trajectory of the zeros and poles of the M matrix.

Using the computed $\mathbf{M}_o$ at the series of R values considered here, we then extracted partial widths for the resonance for decaying into the $s\sigma_g$ and $d\sigma_g$ channels using the multichannel extension of the Breit-Wigner form.[24,38] Morales et $al.$[31] also calculated partial widths using a
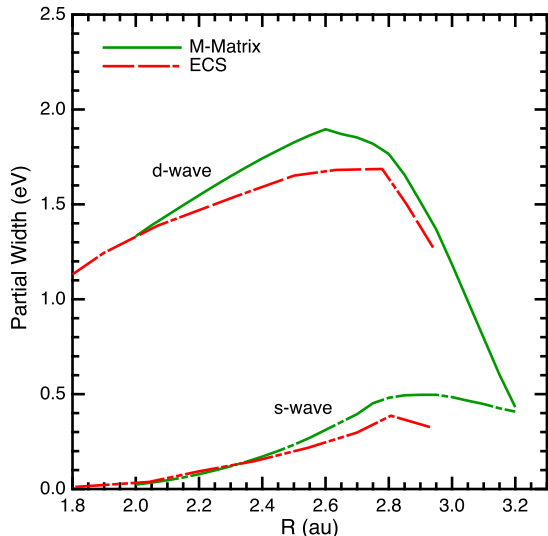
Figure 16: Partial widths of the $^1\Sigma_g^+$ resonant state of the e-H_2^+ system extracted from $\mathbf{M}_o$ as a function $R_{\text{H-H}}$. Both the widths for decay into the $s\sigma_g$ and $d\sigma_g$ channels are given. Our results are compared to the partial widths computed using Feshbach projection from Ref.[31]

Feshbach projection operator method and in Fig. 16 our computed partial widths are presented and are compared to those of.[31] In these fits to extract the partial widths, the total width was not constrained to exactly match the width obtained from the zeros and poles of the $\mathbf{M}_o$ matrix. We found that the total width from the Breit-Wigner fits differed from the width from the zeros and poles in $\mathbf{M}_o$ with a root-mean-square error of 0.1 eV. The present results exhibit the same behavior as was found in the Feshbach projection results, with the $s\sigma_g$ being much smaller than the $d\sigma_g$ width for positive energies. Using the $\mathbf{M}_o$ matrix continuation to the bound spectrum, we find that the $s\sigma_g$ width approaches the $d\sigma_g$ at negative energy.

5   Conclusion

We have seen that in the case of a scattering problem with a long-range Coulomb potential, the widths of resonances in the scattering do not go to zero as the resonance moves below the scattering threshold. In the complex k-plane the poles in the S-matrix, which correspond to scattering resonances, do not smoothly connect with poles that correspond to bound states. In analogy with the standard quantum-defect theory, we have defined an M-matrix from which the bound state energies can be extracted and which smoothly connects with the S-matrix above threshold. This M-matrix is obtained using an alternative pair of linearly independent pair of Coulomb functions. An analysis of the behavior of the M matrix shows that it agrees with the S matrix above threshold and has the same pole and zero structure at positive energies. Below threshold the poles and zeros in S^{SR} have been removed in the definition of the M-matrix and the resulting quantum defects are seen to have a Breit-Wigner like behavior in the presence of a resonant state. We have also presented a multichannel extension of the one-channel M-matrix which has analytic properties very similar to the one channel version.

Although the procedures, discussed in the Introduction, for obtaining resonance resonances parameters for neutral molecules using partial charges may give useful results,[17–20] there is no analytic connection between any bound states poles in the presence of a long-range Coulomb potential and resonant states above threshold.

The introduction of the M-matrix provides a way to parameterize the behavior of the Rydberg energy levels at negative energies and scattering S-matrices at positive energies using the same functional form. Considering two prototypical examples, we have seen how combined fits of scattering and bound state data can be performed in both single channel and multichannel cases. The same ideas in principle allow the practical reconstruction via analytic continuation of the motion of the poles of the S-matrix from the behavior of quantum defects alone, at least near the relevant scattering thresholds.

National Energy Research Scientific Computing Center, a DOE Office of Science User Facility.

A Coulomb functions

The regular Coulomb function we use here is defined as in references,[2,39,40] and in terms of the Whittaker function,[22] $M_{\kappa,\mu}(z)$, it is

$$
\begin{aligned}
F_l(k,r) = & \\
\frac{e^{-\pi n/2}|\Gamma(l+1+in)|}{2(2l+1)!}&(\mp i)^{l+1}M_{\pm in,l+1/2}(\pm 2ikr) \\
\to \sin(kr - n\ln 2kr &- l\pi/2 + \eta_l)
\end{aligned}
\tag{49}
$$

where the Coulomb phase shift is

$$
\eta_l = \arg\Gamma(l+1+in) \tag{50}
$$

and

$$
n \equiv \frac{Z}{k}, \tag{51}
$$

where $Z = Z_1 Z_2$, where Z_1 and Z_2 are the charges in units of e of the two interacting particles so that for an electron and an atom with charge of $+1$, $Z = -1$.

One pair of linearly-independent outgoing and incoming Coulomb functions, which we will use, are $H_l^\pm(n,kr)$ and are defined[40] in terms of Whittaker W function[22] as

$$
\begin{aligned}
H_l^\pm(k,r) = (\mp i)^l e^{(\pi n/2)\pm i\eta_l}&W_{\mp in,l+1/2}(\mp 2ikr) \\
\to \exp[\pm(kr - n\ln 2kr &- l\pi/2 + \eta_l)].
\end{aligned}
\tag{52}
$$

Note that $W_{\kappa,\mu}(z)$ has a term that depends on $\ln(z)$ so that it is a many-valued function. As a consequence, care must by exercized when considering the analytic continuation of these functions, in particular in choosing the correct branch when crossing the branch cuts in the definition of W.

A related pair of linearly-independent Coulomb functions, $f_l^\pm(k,r)$,[39] are defined as

$$
f_l^\pm(k,r) = (\pm)^l \exp(\mp \eta_l(k)) H_l^\pm(Z/k,kr) \tag{53}
$$

so that $f_l^\pm(k,r)$ can be written

$$
\begin{aligned}
f_l^+(k,r) &= e^{\frac{\pi n}{2}}W_{-in,l+\frac{1}{2}}(-2ikr) \quad (54) \\
f_l^-(k,r) &= e^{\frac{\pi n}{2}}W_{+in,l+\frac{1}{2}}(+2ikr). \quad (55)
\end{aligned}
$$

These Coulomb functions can be analytically continued to complex values of k as discussed by Thompson and Barnett.[41]

References

(1) Newton, R. G. *Scattering theory of waves and particles, second edition*; Springer-Verlag Inc.: New York, NY, 1982.

(2) Taylor, J. R. *Scattering theory: The quantum theory of nonrelativistic collisions*; Dover Publications, Inc: Mineola, New York, 1972, 2006; p 238 ff.

(3) Giusti, A. A multichannel quantum defect approach to dissociative recombination. *Journal of Physics B: Atomic and Molecular Physics* **1980**, *13*, 3867.

(4) Guberman, S. L.; Giusti-Suzor, A. The generation of O(^{1}S) from the dissociative recombination of O$_2^+$. *The Journal of Chemical Physics* **1991**, *95*, 2602–2613.

(5) Guberman, S. L. Dissociative recombination without a curve crossing. *Phys. Rev. A* **1994**, *49*, R4277–R4280.

(6) Kokoouline, V.; Greene, C. H.; Esry, B. D. Mechanism for the destruction of H$_3^+$ ions by electron impact. *Nature* **2001**, *412*, 891–894.

(7) Kokoouline, V.; Curik, R.; Greene, C. H. Non-adiabatic effects in dissociative recombination of molecular ions. *Journal of Physics: Conference Series* **2009**, *192*, 012017.

(8) Jungen, C.; Pratt, S. T. Low-energy dissociative recombination in small polyatomic molecules. *The Journal of Chemical Physics* **2010**, *133*, 214303.

(9) Niyonzima, S.; Lique, F.; Chakrabarti, K.; Larson, Å.; Orel, A. E.; Schneider, I. F. Multichannel-quantum-defect-theory treatment of reactive collisions between electrons and BeH^+. *Phys. Rev. A* **2013**, *87*, 022713.

(10) dos Santos, S. F.; Ngassam, V.; Orel, A. E.; Larson, Å. Dissociative recombination of N_2H^+. *Phys. Rev. A* **2016**, *94*, 022702.

(11) Domcke, W. Analytic theory of resonances and bound states near Coulomb thresholds. *Journal of Physics B: Atomic and Molecular Physics* **1983**, *16*, 359.

(12) Miller, W. H.; Morgner, H. A unified treatment of Penning ionization and excitation transfer. *The Journal of Chemical Physics* **1977**, *67*, 4923–4930.

(13) Seaton, M. J. Quantum defect theory I. General formulation. *Proceedings of the Physical Society* **1966**, *88*, 801.

(14) Seaton, M. J. Quantum defect theory. *Reports on Progress in Physics* **1983**, *46*, 167.

(15) Chernov, V. E.; Manakov, N. L.; Starace, A. F. Exact analytic relation between quantum defects and scattering phases with applications to Green's functions in quantum defect theory. *The European Physical Journal D* **2000**, *8*, 347–359.

(16) Fonseca dos Santos, S.; Douguet, N.; Kokoouline, V.; Orel, A. E. Scattering matrix approach to the dissociative recombination of HCO^+ and N_2H^+. *The Journal of Chemical Physics* **2014**, *140*, 164308.

(17) Nestmann, B.; Peyerimhoff, S. D. Calculation of the discrete component of resonance states in negative ions by variation of nuclear charges. *Journal of Physics B: Atomic and Molecular Physics* **1985**, *18*, 615.

(18) Nestmann, B. M.; Peyerimhoff, S. D. CI method for determining the location and width of resonances in electron-molecule collision processes. *Journal of Physics B: Atomic and Molecular Physics* **1985**, *18*, 4309.

(19) Horáček, J.; Paidarová, I.; Čurík, R. On a simple way to calculate electronic resonances for polyatomic molecules. *The Journal of Chemical Physics* **2015**, *143*, 184102.

(20) Čurík, R.; Paidarová, I.; Horáček, J. The $^2\Pi_g$ shape resonance of acetylene anion: an investigation with the RAC method. *The European Physical Journal D* **2016**, *70*, 1–6.

(21) White, A. F.; Head-Gordon, M.; McCurdy, C. W. Stabilizing potentials in bound state analytic continuation methods for electronic resonances in polyatomic molecules. *The Journal of Chemical Physics* **2017**, *146*, 044112.

(22) Olver, F. W. J., Lozier, D. W., Boisvert, R. F., Clark, C. W., Eds. *NIST Handbook of Mathematical Functions*; Cambridge University Press: New York, NY, 2010; p 321 ff.

(23) Seaton, M. J. Thermal Inelastic Collision Processes. *Reviews of Modern Physics* **1958**, *30*, 979–991.

(24) Hazi, A. U. Behavior of the Eigenphase Sum Near a Resonance. *Phys. Rev. A* **1979**, *19*, 920–922.

(25) Newton, R. G. *Scattering theory of waves and particles*; Springer-Verlag Inc.: New York, NY, 1982; p 528 ff.

(26) Guberman, S. L. Potential curves for dissociative recombination of O_2^+. *International Journal of Quantum Chemistry* **1979**, *16*, 531–540.

(27) Dunning Jr., T. H. Gaussian basis functions for use in molecular calculations. I. Contraction of ($9s5p$) atomic basis sets for

the first-row atoms. *J. Chem. Phys.* **1970**, *53*, 2823–2833.

(28) Rescigno, T. N.; Lengsfield III, B. H.; McCurdy, C. W. In *Modern electronic structure theory*; Yarkony, D. R., Ed.; World Scientific: Singapore, 1995; Vol. I; Chapter 9, pp 501–588.

(29) Greene, C. H.; Jungen, C. Molecular Applications of Quantum Defect Theory. *Advances in Atomic and Molecular Physics* **1985**, *21*, 51–121.

(30) Shimamura, I.; Noble, C. J.; Burke, P. G. Complex quantum defects of superexcited Rydberg states of H_2. *Physical Review A* **1990**, *41*, 3545–3554.

(31) Morales, F.; McCurdy, C. W.; Martn, F. Validity of the isolated resonance picture for H_2 autoionizing states. *Physical Review A* **2006**, *73*, 014702.

(32) Ross, S. C.; Jungen, C. Multichannel quantum-defect theory of double-minimum $^1\Sigma_g^+$ states in H_2. I. Potential-energy curves. *Physical Review A* **1994**, *49*, 4353–4363.

(33) Dunning, J., Thom H. Gaussian basis sets for use in correlated molecular calculations. I. The atoms boron through neon and hydrogen. *Journal of Chemical Physics* **1989**, *90*, 1007–1023.

(34) Kendall, R. A.; Dunning, J., Thom H.; Harrison, R. J. Electron affinities of the first-row atoms revisited. Systematic basis sets and wave functions. *Journal of Chemical Physics* **1992**, *96*, 6796–6806.

(35) Kaufmann, K.; Baumeister, W.; Jungen, M. Universal Gaussian basis sets for an optimum representation of Rydberg and continuum wavefunctions. *Journal of Physics B: Atomic, Molecular and Optical Physics* **1989**, *22*, 2223–2240.

(36) Stratmann, R. E.; Lucchese, R. R. A graphical unitary group approach to study multiplet specific multichannel electron correlation effects in the photoionization of O_2. *Journal of Chemical Physics* **1995**, *102*, 8493–8505.

(37) Stratmann, R. E.; Zurales, R. W.; Lucchese, R. R. Multiplet-specific multichannel electron-correlation effects in the photoionization of NO. *Journal of Chemical Physics* **1996**, *104*, 8989–9000.

(38) Rescigno, T. N.; Trevisan, C. S.; Orel, A. E.; Slaughter, D. S.; Adaniya, H.; Belkacem, A.; Weyland, M.; Dorn, A.; McCurdy, C. W. Dynamics of dissociative electron attachment to ammonia. *Physical Review A* **2016**, *93*, 052704.

(39) Newton, R. G. *Scattering theory of waves and particles*; Springer-Verlag Inc.: New York, NY, 1982; p 424 ff.

(40) Olver, F. W. J., Lozier, D. W., Boisvert, R. F., Clark, C. W., Eds. *NIST Handbook of Mathematical Functions*; Cambridge University Press: New York, NY, 2010; p 741 ff.

(41) Thompson, I. J.; Barnett, A. R. Coulomb and Bessel Functions of Complex Arguments and Order. *J. Comp. Phys.* **1986**, *64*, 490–509.

Graphical TOC Entry

Resonance pole and zero in the analytically continued quantum defect matrix with their trajectories.